

R. Nandan<sup>a</sup>, T. J. Lienert<sup>b</sup>, T. DebRoy<sup>a</sup>

<sup>a</sup> The Pennsylvania State University, Department of Materials Science and Engineering, PA, USA

<sup>b</sup> Los Alamos National Laboratory, Materials Science and Technology, Los Alamos, NM, USA

# Toward reliable calculations of heat and plastic flow during friction stir welding of Ti-6Al-4V alloy

*Dedicated to Professor Dr. Horst Cerjak on the occasion of his elevation to Emeritus status*

Heat transfer and visco-plastic flow during friction stir welding of Ti-6Al-4V alloy have been modeled in three dimensions by numerically solving the equations of conservation of mass, momentum and energy using temperature dependent thermo-physical properties and temperature and strain-rate dependent viscosity values. The computed results showed that five important model parameters, i.e., the spatially variable friction coefficient, the spatially variable slip between the tool and the workpiece, the extent of viscous dissipation, the mechanical efficiency and the spatially variable heat transfer rate from the bottom surface of the workpiece significantly affected both the temperature fields and the computed torque on the tool. An important problem in the modeling of friction stir welding is that the values of these five parameters cannot be specified from fundamental principles and, as a result, computed results are not always accurate. Here we show that by combining the heat transfer and plastic flow model with a genetic algorithm based optimization scheme, the values of the five uncertain parameters can be determined from a limited volume of experimental data so that the model predictions of peak temperatures and cooling rates match well with the experimental results. The computed results show that for the welding conditions reported in this paper, close to sticking condition prevailed at the tool-workpiece interface for all the experiments. The extent of viscous dissipation converted to heat was fairly low indicating lack of intimate atomic mixing in the stir zone. Computed three dimensional pressure distributions and streamlines were consistent with defect-free reliable welds for all conditions of welding studied.

**Keywords:** Torque; Heat generation rate; Boundary conditions; Genetic algorithm; Computational modeling

## 1. Introduction

Friction stir welding (FSW) is a solid-state joining process, in which a cylindrical or conical threaded pin, mounted on a larger diameter shoulder, is inserted between two rigidly clamped plates, and rotated at high speeds as it moves along the joint interface. Sufficient load is applied on the tool to keep the shoulder in contact with the top surface of the workpiece. The heat generated by friction plasticizes the

workpiece material near the tool, transporting it from the front to the back of the tool and forming the welded joint. Although FSW was originally developed for aluminum alloys [1], it has now been used for the welding of steels and a variety of other important engineering alloys such as Ti-6Al-4V. This titanium alloy is widely used in aerospace, chemical and other industries due to its high specific strength and low susceptibility to corrosion. FSW is a potentially attractive joining technique for this alloy especially because conventional fusion welding often leads to problems resulting from reaction with ambient gases at elevated temperatures. However, because FSW is relatively new, our understanding of it, and particularly FSW of Ti-6Al-4V is still developing.

In fusion welding, numerical models [2, 3] have provided significant insight into the welding processes and welded materials that could not have been obtained otherwise. Starting with the calculation of temperature and velocity fields, these models have been used to understand weld pool shape and size [2, 3], solidified surface profiles and cooling rates, [3] solidification characteristics [2–4], grain structure [5] and topology [6], phase transformation kinetics [7], inclusion type and size distribution [8], vapor composition [9], plasma characteristics [10], weld metal composition change [11] and for the prevention of several types of weld defects [12, 13]. In the last several years several computational models of FSW have been proposed [14–27]. However, these models have not been widely used, especially in industry. A major problem is that most phenomenological models are complex and they contain many uncertain parameters that cannot be determined from fundamental principles [17]. Most models do not have any structural component to ensure that the model predictions agree well with the experimental results. This difficulty has been recently recognized in the fusion welding literature. It is now known [28–30] that the reliability of the results obtained from the heat and materials flow models can be enhanced by optimizing values of several uncertain input parameters using a limited volume of experimental data.

The main components of any phenomenological heat transfer and plastic flow model of FSW are the equations of conservation of mass, momentum and energy. Any lack of reliability in phenomenological models originates from the specification of boundary conditions or other auxiliary components of the model. These include quantitative description of the spatially variable heat transfer rate from

the bottom surface of the workpiece, incomplete knowledge about the extent of slip between the tool and the workpiece, and the uncertainties about the spatially variable friction coefficient and other parameters. It is important to use accurate values of any model parameter that can affect the computed results significantly. An appropriate sensitivity study using a phenomenological model can reveal the impact of the chosen values of any parameter that is necessary but cannot be determined from fundamental principles. For example, if important features of FSW such as the peak temperature, thermal cycles, and the torque are sensitive to the values of several model parameters whose values cannot be prescribed accurately, the uncertainty in the values of these parameters would adversely affect the modeling results. A phenomenological model must have a mechanism to determine the optimized values of these uncertain input parameters within the framework of the fundamental laws, so that the computed results agree with the corresponding experimental results to the maximum extent possible.

Here we use a version of genetic algorithm, differential evolution [31, 32], to determine the optimized values of five uncertain parameters from a limited volume of experimental results. We identify these parameters based on the results of a sensitivity study that showed that the spatially variable friction coefficient, the position-dependent slip between the tool and the workpiece, the extent of viscous dissipation, the mechanical efficiency and the spatially variable heat loss rate from the bottom surface of the workpiece to its environment significantly affected both the computed temperature fields and torque on the tool. Therefore the values of these parameters were optimized using a limited volume of measured temperatures at several monitoring locations during FSW of Ti-6Al-4V. Using the optimized values of the parameters, the computed values of the peak temperatures at several monitoring locations and the time spans at the base of the thermal cycles at several monitoring locations were compared with the corresponding experimentally measured values. Apart from providing a detailed insight into the heat transfer and materials flow in the workpiece, the computed results also reveal the extent of slip at the tool-workpiece interface and the extent of viscous dissipation converted to heat for all the experiments. Computed three dimensional pressure distributions and streamlines were examined in the context of defect-free reliable welds for all conditions of welding studied.

## 2. Materials and experiments

Friction stir welds were produced on plates (7.2 mm × 102 mm × 203 mm) of a Ti-6Al-4V alloy in the mill annealed condition. The composition of the specific alloy was: 6.4% Al, 3.85% V, 0.22% Fe, 0.18% O and 0.013% H (all wt.%) with the balance Ti. The plates were rigidly held in a butt weld configuration for joining. The pin was 6.4 mm in length and 7.9 mm in diameter. This tool/workpiece combination resulted in partial-penetration welds. The pin was not tapered and did not feature any threads or other profiling. The tool was machined from commercially pure (CP) tungsten. Initial screening experiments were performed to develop optimized weld parameters. Optimized welds were made using a tool with a 19 mm diameter shoulder at travel speeds of 1.6 mm s<sup>-1</sup> and a tool rotation rate of 275 rpm.

The welding direction was parallel to the rolling direction of the plate. The tool and workpiece were protected from surface oxidation by welding in an inert gas chamber with a sliding top section made of clear plexi-glass. Axial loads and torques on the tool were determined during each weld using a calibrated strain gage set attached to the tool holder. For each weld, type K thermocouples were attached at several locations on the top (12.2 mm from the weld-centerline in the retreating side) and bottom surfaces (3.2 mm from the weld centerline on both advancing and retreating sides) of the workpiece. After welding, features on each weld were correlated with the temperature, load and torque signals.

## 3. Mathematical model

### 3.1. Heat transfer and plastic flow

A schematic diagram of the computational domain is shown in Fig. 1. It includes the workpiece and the tool pin inserted inside the workpiece. However, it does not include the tool shoulder. The dimensions of the plate and the tool used and the thermo-physical properties of the workpiece and the tool material are given in Table 1. Between warm-up after pin-insertion and pin-extraction from the workpiece, the thermal cycles at locations equidistant from the weld centerline were similar and the torque values measured at different instances were almost constant. Therefore, the temperature and velocity fields were solved assuming steady state behavior. The plastic flow in a three dimensional cartesian coordinate system is represented by the momentum conservation equation in index notation, with *i* or *j* = 1, 2 and 3, representing *x*, *y* and *z* directions, respectively [16, 19, 21]:

$$\rho \frac{\partial u_i u_j}{\partial x_i} = - \frac{\partial p}{\partial x_j} + \frac{\partial}{\partial x_i} \left( \mu \frac{\partial u_j}{\partial x_i} + \mu \frac{\partial u_i}{\partial x_j} \right) - \rho U_1 \frac{\partial u_j}{\partial x_1} \quad (1)$$

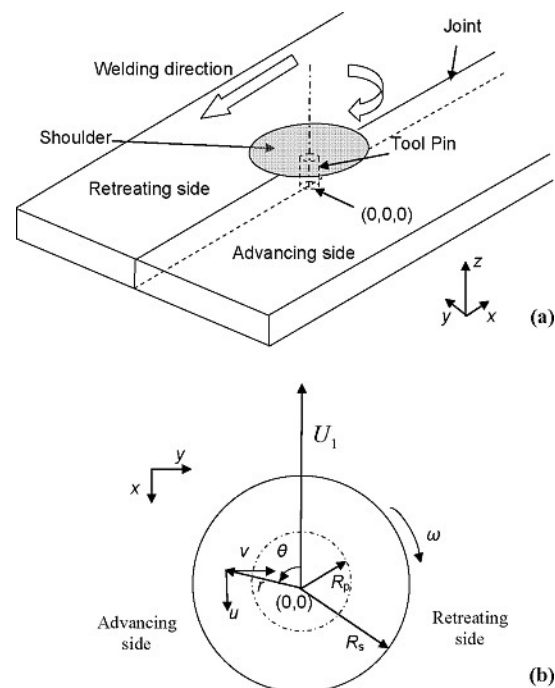


Fig. 1. (a) A schematic diagram of the FSW system considered in the model. (b) Top view of the rotating tool moving in the negative *x*-direction.  $\theta = 0$  corresponds to plane  $y = 0$ ,  $x < 0$ .

Table 1. Data used in the FSW calculations.

Property/Weld parameter	Value
Workpiece length ( <i>x</i> -direction)	0.33 m
Workpiece half-width ( <i>y</i> -direction)	0.10 m
Workpiece thickness	7.2 mm
Shoulder radius	9.5 mm
Pin radius	3.95 mm
Pin length	6.4 mm
Pitch of the thread	1.0 mm
Weld speed	1.6 mm s <sup>-1</sup>
Rotational speed	275 rpm
Axial pressure	60.0 MPa
Tilt angle	0°
Work piece material	Ti-6Al-4V
Density	4420 kg m <sup>-3</sup>
Specific heat capacity [37], <i>C<sub>p</sub></i>	J kg <sup>-1</sup> K <sup>-1</sup>
622 - 0.367 <i>T</i> + 5.45 × 10 <sup>-4</sup> <i>T</i> <sup>2</sup> + 2.39 × 10 <sup>-8</sup> <i>T</i> <sup>3</sup>	
Thermal conductivity [37], <i>k</i>	W m <sup>-1</sup> K <sup>-1</sup>
1.92 + 1.89 × 10 <sup>-2</sup> <i>T</i> - 1.53 × 10 <sup>-5</sup> <i>T</i> <sup>2</sup> + 1.41 × 10 <sup>-8</sup> <i>T</i> <sup>3</sup>	
Tool	Tungsten
Density	19400 kg m <sup>-3</sup>
Specific heat capacity [36], <i>C<sub>p</sub></i>	J kg <sup>-1</sup> K <sup>-1</sup>
128.3 - 3.279 × 10 <sup>-2</sup> <i>T</i> + 3.41 × 10 <sup>-6</sup> <i>T</i> <sup>2</sup>	
Thermal conductivity [36], <i>k</i>	W m <sup>-1</sup> K <sup>-1</sup>
153.5 - 9.56 × 10 <sup>-2</sup> <i>T</i> + 5.23 × 10 <sup>-5</sup> <i>T</i> <sup>2</sup>	

where *u* is the velocity, *ρ* is the density, *μ* is the non-Newtonian viscosity, *U*<sub>1</sub> is the welding velocity, and *p* is the pressure. Viscosity can be determined from flow stress and effective strain rate as follows [33]:

$$\mu = \frac{\sigma_e}{3\dot{\epsilon}} \quad (2)$$

The calculation of viscosity requires local values of strain rate and temperature. The viscosity was calculated based on the following formulation of flow stress, *σ<sub>e</sub>*, proposed by Sheppard and Wright [34]:

$$\sigma_e = \frac{1}{\alpha} \sinh^{-1} \left[ \left( \frac{Z}{A} \right)^{1/n} \right] \quad (3)$$

where *A*, *a*, and *n* are material constants and *Z* is the Zener–Hollomon parameter. The value of constants *A* = 2.25 × 10<sup>21</sup> s<sup>-1</sup>, *a* = 0.0066 MPa<sup>-1</sup>, and *n* = 5 [35]. The Zener–Hollomon parameter, *Z*, represents the temperature compensated effective strain rate and is given by:

$$Z = \dot{\epsilon} \exp \left( \frac{Q}{RT} \right) \quad (4)$$

Here *Q* = 501 kJ mol<sup>-1</sup> [34] is the temperature-independent activation energy, *R* is the universal gas constant, *ε̇* is the effective strain rate and is given by

$$\dot{\epsilon} = \left( \frac{2}{3} \epsilon_{ij} \epsilon_{ij} \right)^{\frac{1}{2}} \quad (5)$$

where *ε<sub>ij</sub>* is the strain rate tensor, defined as

$$\epsilon_{ij} = \frac{1}{2} \left( \frac{\partial u_i}{\partial x_j} + \frac{\partial u_j}{\partial x_i} \right) \quad (6)$$

Finally, viscosity can be determined from the flow stress and effective strain rate using Eq. (2). Contours of viscosity are shown in Fig. 2. It shows high sensitivity to temperature at high strain-rates. The pressure field was obtained by solving the following continuity equation iteratively with the momentum equations for incompressible single phase flow.

$$\frac{\partial u_i}{\partial x_i} = 0 \quad (7)$$

where *u<sub>i</sub>* is the velocity of plastic flow. The steady single-phase momentum conservation equations with reference to

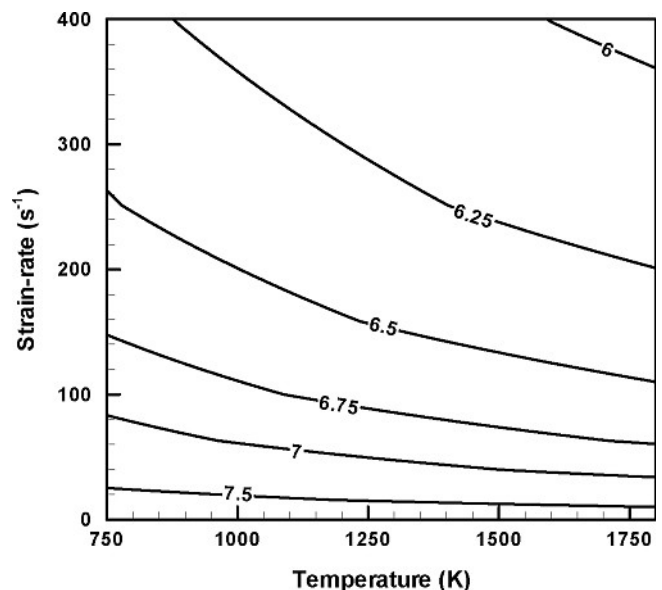


Fig. 2. Plot showing computed contours of viscosity as a function of strain rate and temperature. The contour labels represent log<sub>10</sub>(viscosity in Pa s).

a co-ordinate system attached to the heat source may be represented as [16, 19, 21]:

$$\rho C_p \frac{\partial(u_i T)}{\partial x_i} = -\rho C_p U_1 \frac{\partial T}{\partial x_1} + \frac{\partial}{\partial x_i} \left( k \frac{\partial T}{\partial x_i} \right) + S_{in} + S_b \quad (8)$$

where  $C_p$  is the specific heat and  $k$  is the temperature-dependent thermal conductivity of the workpiece/tool [36, 37]. The term  $S_{in}$  represents the source term due to interfacial heat generation rate per unit volume at the tool pin-work piece interface and  $S_b$  is the heat generation rate due to plastic deformation in the workpiece away from the interface. The heat generated at the interface between vertical and horizontal surfaces of the tool pin and the workpiece may be defined as [16, 19, 21]:

$$S_{in} = [(1 - \delta) \eta \tau + \delta \mu_f P_N] (\omega r - U_1 \sin \theta) \frac{A_r}{V} \quad (9)$$

where,  $A_r$  is any small area on the tool pin-work piece interface,  $r$  is the radial distance of the center of the area from the tool axis,  $V$  is the control-volume enclosing the area  $A_r$ ,  $\tau$  is the maximum shear stress at yielding and  $\theta$  is the angle with the negative  $x$ -axis in the counter-clockwise direction,  $\eta$  is the mechanical efficiency, i.e. the amount of mechanical energy converted to heat energy,  $\delta$  denotes the spatially variable fractional slip between the tool and the workpiece interface,  $\mu_f$  is the spatially variable coefficient of friction,  $\omega$  is the angular velocity,  $P_N$  is the normal pressure on the surface and is equal  $P_V$  for the workpiece area in contact with the vertical surface of the pin and is equal to  $P_H$  for area below the horizontal surface of the tool. Full sticking is indicated by  $\delta = 0$ . The velocity  $(\omega r - U_1 \sin \theta)$  represents the local velocity of a point on the tool with the origin fixed at the tool-axis. The normal pressure on the workpiece top surface has been assumed to be same at all places in contact with the tool shoulder. In Eq. (9) the applied radial pressure is much smaller than the applied axial pressure and the value of  $P_V$  has been assumed to be zero.

An estimate of the viscous dissipation of momentum per unit volume,  $S_b$ , has been calculated as  $\varepsilon \mu \Phi$  where  $\Phi$  is given by:

$$\Phi = 2 \sum_{i=1}^3 \left( \frac{\partial u_i}{\partial x_i} \right)^2 + \left( \frac{\partial u_1}{\partial x_2} + \frac{\partial u_2}{\partial x_1} \right)^2 + \left( \frac{\partial u_1}{\partial x_3} + \frac{\partial u_3}{\partial x_1} \right)^2 + \left( \frac{\partial u_3}{\partial x_2} + \frac{\partial u_2}{\partial x_3} \right)^2 \quad (10)$$

and  $\varepsilon$  is an arbitrary constant that indicates the extent of mixing on the atomic scale. The value of  $\varepsilon$  may tend to 1 for a well mixed system in molecular scale. In systems where the grains remain largely intact, the value of  $\varepsilon$  may be very small. Here, we try to optimize the value of this parameter so that a good agreement can be obtained between the output of the model and physical experiment, thus improving the reliability and utility of the model.

The total heat generated at the shoulder/workpiece interface has been partitioned between the work piece and the tool in the ratio given below [38]:

$$f = \frac{J_W}{J_T} = \frac{\sqrt{(k\rho C_p)_W}}{\sqrt{(k\rho C_p)_T}} \quad (11)$$

where the subscripts W and T denote the workpiece and the tool, respectively. The analytical expression is based on steady-state one dimensional heat transfer from point heat source located at the interface of dissimilar metals. The heat flux into the work piece is estimated to be 45 % of the total heat generated. This relation has been examined experimentally by Lienert et al. [39] and found to be reliable.

A heat flux continuity at the shoulder matrix interface yields:

$$k \frac{\partial T}{\partial z} \Big|_{\text{top}} = \frac{J_W}{J_W + J_T} q_1 \quad \text{in the range } R_P \leq r \leq R_S \quad (12)$$

$R_P$  and  $R_S$  represent the tool pin and shoulder radius, respectively and  $q_1$  represents the total rate of heat generation at the shoulder-workpiece interface. It is given by:

$$q_1 = [\eta(1 - \delta) \tau + \delta \mu_f P_H] (\omega r - U_1 \sin \theta) \quad (13)$$

At the bottom surface, there is a backing plate and the heat transfer coefficient from the bottom of the workpiece is not the same as for free convection. The value of the heat transfer coefficient was determined by optimization.

$$k \frac{\partial T}{\partial z} \Big|_{\text{bottom}} = h_b (T - T_a) \quad (14)$$

where  $h_b$  is the bottom heat transfer coefficient and  $T_a$  is the ambient temperature of 298 K. The heat transfer coefficient at the bottom face depends on the local temperature and is given by the following relation [40]:

$$h_b = h_{b0} (T - T_a)^{0.25} \quad (15)$$

where  $h_{b0}$  is the heat transfer parameter for the bottom surface. As Eq. (15) shows, this parameter is a constant and it has a different unit than the heat transfer coefficient which is spatially variable. At the top surface, heat transfer is due to both convection and radiation and is given by:

$$k \frac{\partial T}{\partial z} \Big|_{\text{top}} = h_t (T - T_a) + \sigma \varepsilon' (T^4 - T_a^4) \quad (16)$$

$\sigma$  is the Stefan-Boltzmann constant ( $5.67 \times 10^{-16} \text{ J K}^{-4} \text{ m}^{-2} \text{ s}^{-1}$ ),  $\varepsilon$  is the emissivity and  $h_t$  is the convective heat transfer coefficient at the top surface. The computed temperature values were found to be insensitive to the values of  $h_t$  and its value was taken as zero for simplicity. Velocities at the tool pin periphery have been defined in terms of tool translation velocity and the tool pin angular velocity:

$$\begin{aligned} u &= (1 - \delta) (\omega R_P \sin \theta - U_1) \\ v &= (1 - \delta) \omega R_P \cos \theta \end{aligned} \quad (17)$$

Similarly, at the shoulder-work piece interface, the velocity boundary conditions may be written as:

$$\left. \begin{aligned} u &= (1 - \delta) (\omega r \sin \theta - U_1) \\ v &= (1 - \delta) \omega r \cos \theta \end{aligned} \right\} \text{in the range } R_P \leq r \leq R_S \quad (18)$$

At all other surfaces, temperatures are set to ambient temperature (298 K) and the velocities are set to zero.

Table 2. Position of thermocouple, measured peak value and widths of thermal cycles.

Position (R: retreating, A: advancing)	Distance from centerline (mm)	Measured $T_{peak}$ (K)	Calculated $T_{peak}$ (K)	Calculated $L_{773K}$ (mm)	Measured $L_{773K}$ (mm)
1-Back(A)	3.17	1160	1162	21.21	23
2-Back(R)	3.17	1129	1110	19.45	20
3-Top(R)	12.19	813	810	9.72	9.5

The differential equations of continuity and transport were solved using SIMPLE algorithm [41] based solution procedure, capable of calculating three dimensional heat transfer and fluid flow with a stationary or moving heat source, with a free or flat surface, and well tested and used for several welding processes. Typically  $80 \times 80 \times 25$  non-uniform fixed rectangular grid points were used for maximum resolution of variables. The grids were fine near the tool and progressively coarser away from the tool shoulder periphery. The results were verified for grid independence.

The trend of the reported data on the extent of slip during cross-wedge rolling can be expressed by the following relation [42]:

$$\delta = 1 - \exp\left(-\delta_0 \frac{\omega}{\omega_0} \frac{r}{R_S}\right) \quad (19)$$

where  $\delta$  denotes the fraction-slip and  $\delta_0$  is a constant. The above equation was used for all interfaces, with  $r$  denoting the distance of the center of the grid-area from the tool axis. It varies from 0 to  $R_P$  for tool pin's bottom surface, is constant at  $R_P$  for the vertical surface of the pin, and varies from  $R_P$  to  $R_S$  for the tool shoulder-workpiece interface. The normalizing angular velocity,  $\omega_0$ , was taken as  $40 \text{ rad s}^{-1}$ . The value of  $\delta_0$  was optimized from a limited volume of experimental data. This equation embodies the physical picture of the extent of slip increasing with increase in relative velocity between the tool and the workpiece.

Values of friction coefficient were calculated considering the relative velocity between the tool and the workpiece guided by previous work in the field of friction welding of steel bars [43]. The relative velocity increases from zero at the axis of rotation (static condition) to  $\omega R_S$  at the periphery of the tool shoulder (dynamic condition). Experimental evidence suggests [43] that  $\mu_f$  has the following form:

$$\mu_f = \mu_0 \exp\left(-\delta \frac{\omega}{\omega_0} \frac{r}{R_S}\right) \quad (20)$$

where  $\delta$  is the extent of sticking expressed as a fraction and  $r$  is the radial distance from the tool axis for the point in consideration. This equation implies that the friction coefficient decreases with decrease in the relative velocity between the tool and the workpiece.

### 3.2. Optimization of uncertain FSW parameters

Among the necessary input variables in the FSW model, there are five uncertain input parameters that affect the reliability of the model output. These parameters are the heat transfer coefficient at the bottom face of the workpiece ( $h$ ), the spatially variable slip between the tool and the

workpiece interface ( $\delta$ ), the spatially variable coefficient of friction ( $\mu_f$ ), the extent of the viscous dissipation term ( $\epsilon$ ) which indicates degree of atomic mixing in the system and  $\eta$  the mechanical efficiency, the amount of mechanical energy converted to heat energy. In order to optimize the values of these parameters from a limited volume of experimental data, the following objective function was minimized:

$$O = \sqrt{(1 - M_i^*)^2 + \sum_{i=1}^3 \{(1 - T_i^*)^2 + (1 - L_i^*)^2\}} \quad (21)$$

Subscript  $i$  denotes different monitoring locations indicated in Table 2. Three thermal cycles at these locations were used for optimization of uncertain parameters for experiment done at 275 rpm and welding velocity of  $1.6 \text{ mm s}^{-1}$ . The peak temperature and width of thermal cycle were non-dimensionalized using the following expressions:

$$T^* = \frac{T_{cal}}{T_{ex}}; \quad L^* = \frac{L_{cal}}{L_{ex}}; \quad M^* = \frac{M_{cal}}{M_{ex}} \quad (22)$$

where  $T$  is the peak temperature in the workpiece at a monitoring locations indicated in Table 2,  $L$  is the width of the thermal cycle at 773 K and 573 K for the monitoring location,  $M$  is the torque on the tool and the subscripts cal and ex refer to calculated and experimental values, respectively. The objective function value depends on the choice of the five uncertain parameters.

$$O = f(h_0, \mu_0, \delta_0, \epsilon, \eta) \quad (23)$$

Differential Evolution (DE), a population based optimization technique [31, 32], was used to optimize the uncertain parameters for FSW.

## 4. Results and discussion

### 4.1. Sensitivity of output to model parameters

The sensitivities of the computed values of torque on the tool, peak temperature and cooling time on the five uncertain parameters, identified previously, are examined in Fig. 3a–e. Torque is included in the calculations because it affects material flow. To determine the sensitivity, one variable was varied while the others were kept constant. The constant values were:  $\mu_0 = 0.41$ ,  $\delta_0 = 2.3$ ,  $h_{b0} = 167 \text{ W m}^{-2} \text{ K}^{-5/4}$ ,  $\epsilon = 0.5$  and  $\eta = 0.004$ . These values are approximately the mean in the range of values considered for each variable. The peak temperature and the width of thermal cycle were measured at the top surface at a distance of 12 mm from the weld centerline in the advancing side. Figure 3a shows that the peak temperature and the width

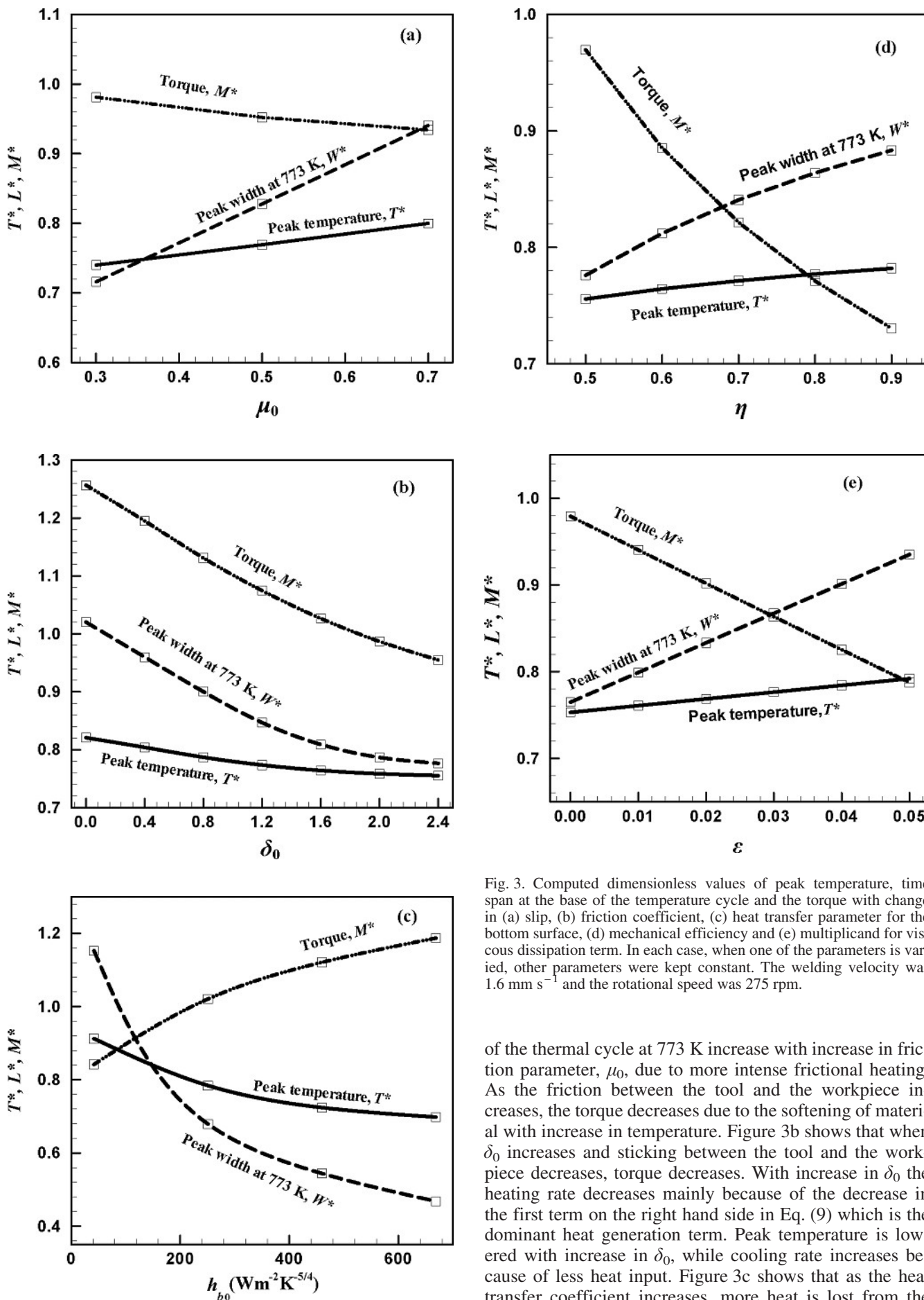


Fig. 3. Computed dimensionless values of peak temperature, time span at the base of the temperature cycle and the torque with change in (a) slip, (b) friction coefficient, (c) heat transfer parameter for the bottom surface, (d) mechanical efficiency and (e) multiplicand for viscous dissipation term. In each case, when one of the parameters is varied, other parameters were kept constant. The welding velocity was  $1.6 \text{ mm s}^{-1}$  and the rotational speed was 275 rpm.

of the thermal cycle at 773 K increase with increase in friction parameter,  $\mu_0$ , due to more intense frictional heating. As the friction between the tool and the workpiece increases, the torque decreases due to the softening of material with increase in temperature. Figure 3b shows that when  $\delta_0$  increases and sticking between the tool and the workpiece decreases, torque decreases. With increase in  $\delta_0$  the heating rate decreases mainly because of the decrease in the first term on the right hand side in Eq. (9) which is the dominant heat generation term. Peak temperature is lowered with increase in  $\delta_0$ , while cooling rate increases because of less heat input. Figure 3c shows that as the heat transfer coefficient increases, more heat is lost from the

Table 3. Optimized sets of uncertain parameters after 180 iterations and the corresponding objective functions, with best set indicated in bold.

Friction coefficient $\mu_0$	Fractional slip $\delta_0$	Heat transfer parameter $h_{b0}$ ( $\text{W m}^{-2} \text{K}^{-5/4}$ )	Mechanical efficiency $\eta$	Efficiency of mixing $\varepsilon$	Objective function $O$
<b>0.7</b>	<b>2.842</b>	<b>418</b>	<b>0.7</b>	<b>0.1</b>	<b>0.469</b>
0.7	2.859	418	0.713	0.1	0.469
0.7	2.833	418	0.751	0.098	0.47
0.7	2.799	418	0.701	0.098	0.471
0.7	2.827	418	0.7	0.099	0.47

workpiece and therefore, the peak temperature and the width of the thermal cycle at 773 K decreases. When the heat transfer coefficient is high, lower temperatures result in harder material and higher torque. Figure 3d and e shows increases in temperature and cooling time with higher values of  $\eta$  and  $\varepsilon$  which represent increases in plastic deformational heat generation at the tool-workpiece interface and inside the workpiece, respectively. More intense heating results in higher temperatures and softer material, resulting in lower torque.

The results in Fig. 3a–e show that all three output variables, peak temperature, time span at the base of the thermal cycle and the torque are sensitive to variations in all the five uncertain input variables. Therefore, all these uncertain input parameters need to be optimized to enhance the reliability of the values of the output variables from the model.

#### 4.2. Optimization of model parameters

The values of the five uncertain input parameters were optimized using the DE technique. For DE, a population of 20 individual sets of five variables was generated. Figure 4 indicates that the average objective function value decreased with successive iterations. The decrease in the objective function was most pronounced during the initial iterations.

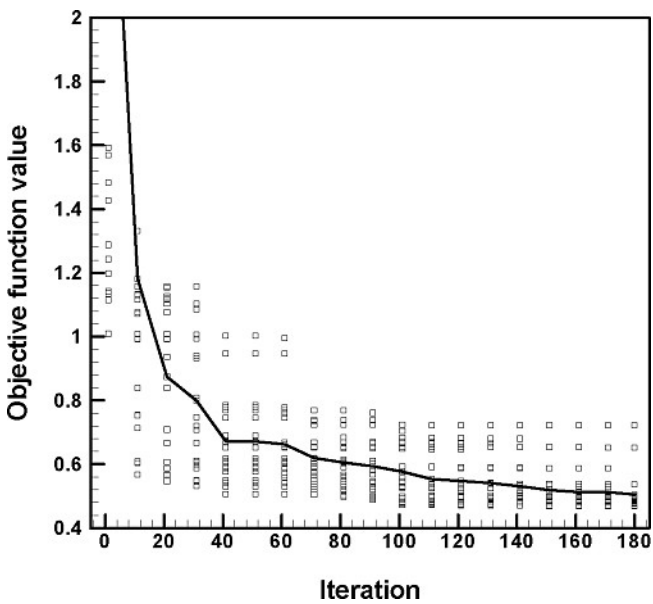


Fig. 4. Objective function value decreases with iteration. The symbols indicate the objective function values for individual sets of variables and the line indicates the change in average value of all individuals with successive iterations.

After 180 iterations, using a mutation factor of 0.8 and a crossover ratio of 0.9, 20 sets of optimized parameter values were obtained. The best five results are given in Table 3. Since DE is elitist, the better solution is always picked during selection; the diversity of the population steadily decreases as shown in Fig. 4.

The large value of  $\delta_0$ , equivalent to very small  $\delta$  value, indicates considerable sticking between the tool and the workpiece even at the shoulder periphery, where tool velocity is highest. The optimized value of heat transfer parameter, defined by Eq. (15), of  $418 \text{ W m}^{-2} \text{K}^{-5/4}$  is high enough to represent considerable heat loss into the backing plate below the workpiece. The resulting heat transfer coefficient value computed using Eq. (15) is of the same order of magnitude as the value reported in the literature for FSW of aluminum alloys [44]. The extent of viscous dissipation,  $\eta$ , is very small, consistent with the fact that mixing is not efficient at the atomic scale. The numerically calculated torque value of 75 N m was within 90 % of the experimentally measured value of 80 N m. The methodology for torque calculation is given in Refs. [16] and [17]. Thus the optimized values of all five uncertain parameters were well within the acceptable range of values for each parameter.

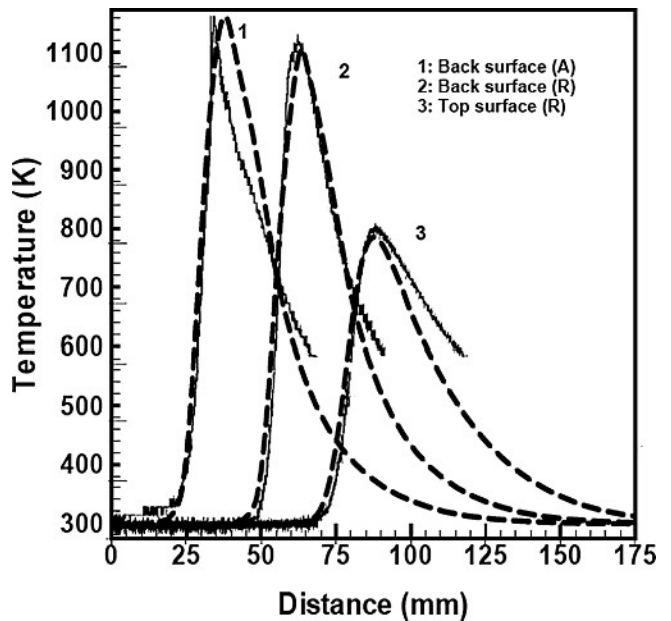


Fig. 5. Comparison between experimental (solid lines) and calculated (dashed lines) temperature profile obtained using optimized parameters:  $\mu_0 = 0.7$ ,  $\delta_0 = 2.842$ ,  $h_{b0} = 418 \text{ W m}^{-2} \text{K}^{-5/4}$ ,  $\eta = 0.7$ ,  $\varepsilon = 0.1$ . Locations 1, 2 and 3 are indicated in Table 2 where the distance is measured from the interface between the two plates. The welding velocity was  $1.6 \text{ mm s}^{-1}$  and the rotational speed was 275 rpm.

Figure 5 shows the computed thermal cycle for the optimized set of parametric values obtained through DE. The objective function was minimized using time spans for thermal cycles corresponding to 773 K and 573 K. Because of the limited volume of experimental data, only two time spans for thermal cycles were included in the objective function that was minimized. A close match between the computed temperature–time variation and the corresponding measured values obtained from the thermocouple can be seen in this figure. The computed average cooling rate in the temperature range of 1173 to 573 K is about  $25 \text{ K s}^{-1}$ , which is well within the range of cooling rates reported for FSW. For the alloy used in the experiments, the oxygen concentration was 0.18 wt.%, and the corresponding  $\beta$ -transus temperature was estimated to be 1254 K from the following equation [45]:

$$T_{\beta\text{-transus}} = 1210 + 242.7 \times (\text{wt.}\% \text{ O}) \quad (24)$$

The computed peak temperature in workpiece was around 1500 K which is well above the  $\beta$ -transus temperature consistent with the observation of prior  $\beta$  grains in the stir zone.

### 4.3. The computed temperature, viscosity and plastic flow fields

The computed temperature profiles along the longitudinal and transverse sections through tool axis and at the top sur-

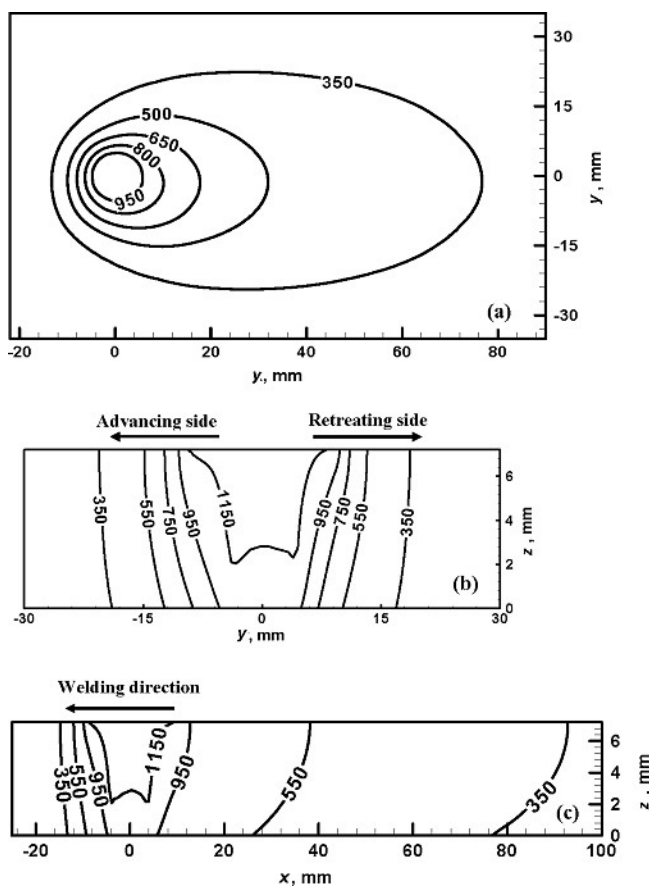


Fig. 6. Computed temperature profiles (K) in (a)  $z = 7.2 \text{ mm}$  ( $xy$ -plane) i.e. top surface of the workpiece, (b)  $x = 0$  ( $yz$ -plane), (c)  $y = 0$  ( $xz$ -plane). The welding velocity was  $1.6 \text{ mm s}^{-1}$  and the rotational speed was 275 rpm.

face of the work piece are shown in Fig. 6a, b and c, respectively. The temperature profiles on the longitudinal mid-section (Fig. 6a) and on the top surface of the work piece (Fig. 6c) are compressed in front of the tool and expanded behind it. The computed results are consistent with the fact that heat is supplied rapidly to the cold region of the work piece ahead of the tool while heat is transported at a lower rate to material already preheated behind the tool. This asymmetry results from the motion of the tool and becomes more prominent at high welding speeds.

Temperature contours and velocity vectors on various horizontal planes are depicted in Fig. 7. The area of plastic flow decreases with distance from the workpiece top surface. The effect of the tool shoulder as a source of momentum is most pronounced in the upper half of the workpiece. The reduction in the area where the flow occurs with distance from the shoulder produces the characteristic shape of the thermo-mechanically affected zone (TMAZ).

Figure 8 shows the stream trace on horizontal planes around the tool pin at three different elevations. The stream lines indicate the presence of nearly circular, closed stream lines indicating recirculating flow of a plug of material around the tool pin. These circular stream lines are consistent with the presence of a layer of plasticized recirculating metal near the pin surface. These closed stream lines occupy larger areas at higher elevations due to greater momentum transport from the rotating shoulder. Beyond the region of recirculating plastic flow, the streamlines indicate that material transfer occurs mainly on the retreating side. Figure 8 also shows a flow separation in the advancing side close to the pin, leading to a relatively stagnant zone, which forms closer to the pin at lower elevations.

The viscosity contours at different horizontal planes,  $z$  values, are shown in Fig. 9. The velocity vectors are also plotted in this figure, superimposed on the viscosity contours. It is observed that the viscosity values in the plastic

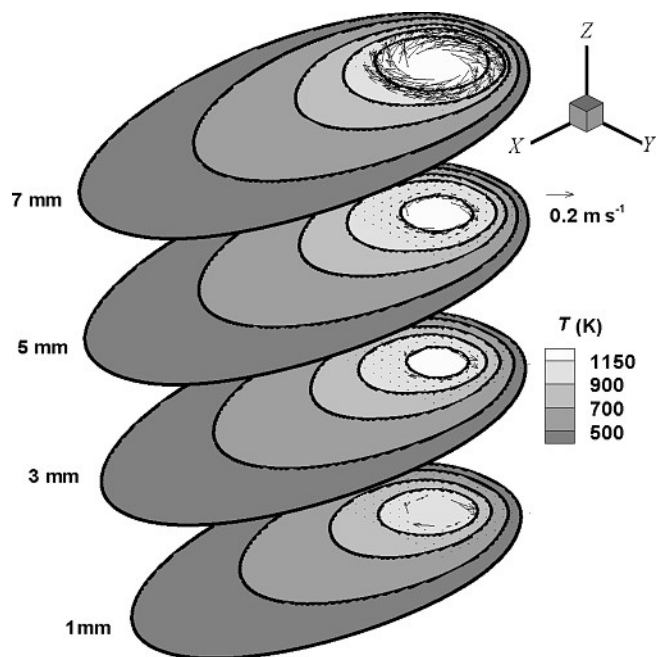


Fig. 7. Temperature contours and velocity vectors at different elevations in the workpiece. The welding velocity was  $1.6 \text{ mm s}^{-1}$  and the rotational speed was 275 rpm.

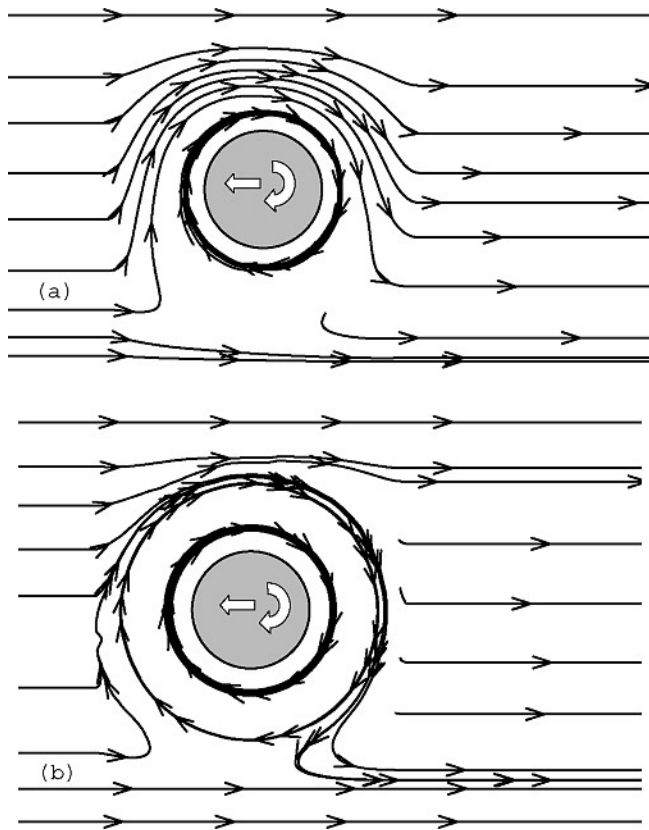


Fig. 8. Streamlines on horizontal planes (a)  $z = 3$  mm and (b)  $z = 7$  mm. The welding velocity was  $1.6 \text{ mm s}^{-1}$  and the rotational speed was 275 rpm.

flow region lie in the range of  $1 \times 10^5$  to  $9.9 \times 10^6$  Pa s. The limiting viscosity beyond which no significant material flow can be observed is found to be  $10^7$  Pa s. The velocity decreases away from the tool pin surface and viscosity increases significantly along that direction. No significant flow occurs when the viscosity is very high. The region of plastic flow decreases with depth.

#### 4.4. Pressure distribution in the flow regime

A careful analysis of the pressure distribution could provide clues about the forging of the plasticized alloy behind the tool and the formation of defects in FSW. Figure 10 shows the distribution of pressure in different horizontal planes. Pressure is higher in front of the tool, as expected, compared to the trailing edge. The pressure distribution is asymmetric about the weld centerline due to asymmetry in the velocity profile. Pressure is somewhat higher on the retreating side than the advancing side. Figure 11 shows pressure distribution in the longitudinal direction in the plane of the weld centerline. The pressure difference between the leading and the trailing edge is higher at lower portions of the tool pin than at points close to the shoulder. This is so because the lower portion of the workpiece experiences lower temperatures and strain-rates and hence has higher flow stress, which physically means that the material is more reluctant to flow and therefore requires higher pressure difference for material flow.

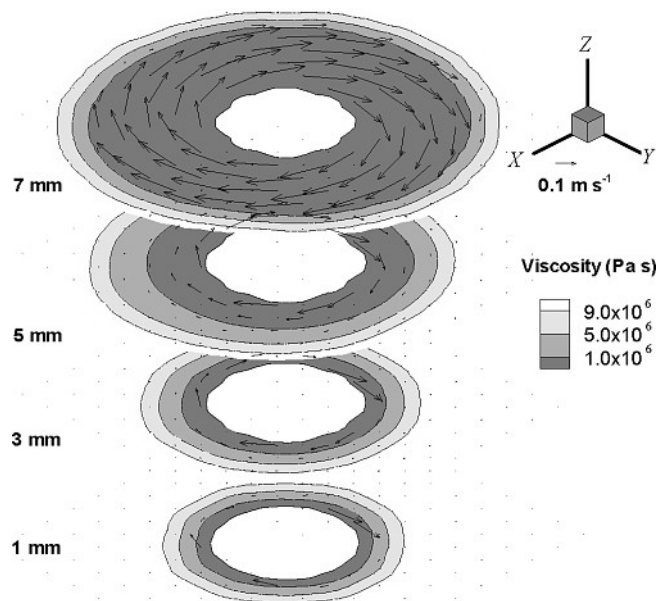


Fig. 9. Plot of spatial variation of velocity at different  $z$ -planes. Near the tool shoulder, the flow field is largest due to momentum transport from the shoulder. The welding velocity was  $1.6 \text{ mm s}^{-1}$  and the rotational speed was 275 rpm.

## 5. Summary and conclusions

Heat and plastic flow during friction stir welding of Ti-6Al-4V alloy was modeled. The model embodied the equations of conservation of mass, momentum and energy coupled with a genetic algorithm model to optimize values of those uncertain model parameters that can significantly affect computed temperature and flow fields. The values of the friction coefficient, the extent of slip between the tool and the workpiece, the heat transfer parameter at the bottom of the workpiece, the mechanical efficiency and the extent of viscous dissipation converted to heat were identified as uncertain input parameters based on a sensitivity study of these variables over appropriate ranges of values. When the values of these five uncertain parameters were optimized using a small volume of experimental data, the computed peak temperature and the thermal cycle agreed well with the corresponding experimental data.

The computed values of the extent of slip indicated considerable sticking between the tool and Ti-6Al-4V alloy at all locations on the tool surface. The computed heat transfer parameter value was found to be  $418 \text{ W m}^{-2} \text{ K}^{-5/4}$  which is consistent with the resulting heat transfer coefficient value reported in the literature for the FSW of aluminum alloys [44]. The small value of the extent of viscous dissipation is consistent with the fact that grains deform plastically but the mixing was not extensive in the plasticized alloy. The peak temperature was found to be about 1500 K consistent with the observed prior beta phase in the stir zone. The computed average cooling rate in the temperature range of 1173 to 573 K was about  $25 \text{ K s}^{-1}$ . The experimentally measured value of torque of about 80 N m was close to the 75 N m value obtained numerically.

This research was supported by a grant from the American Welding Society and Materials Division, Office of Naval Research, Julie A. Christodoulou, Program Officer.

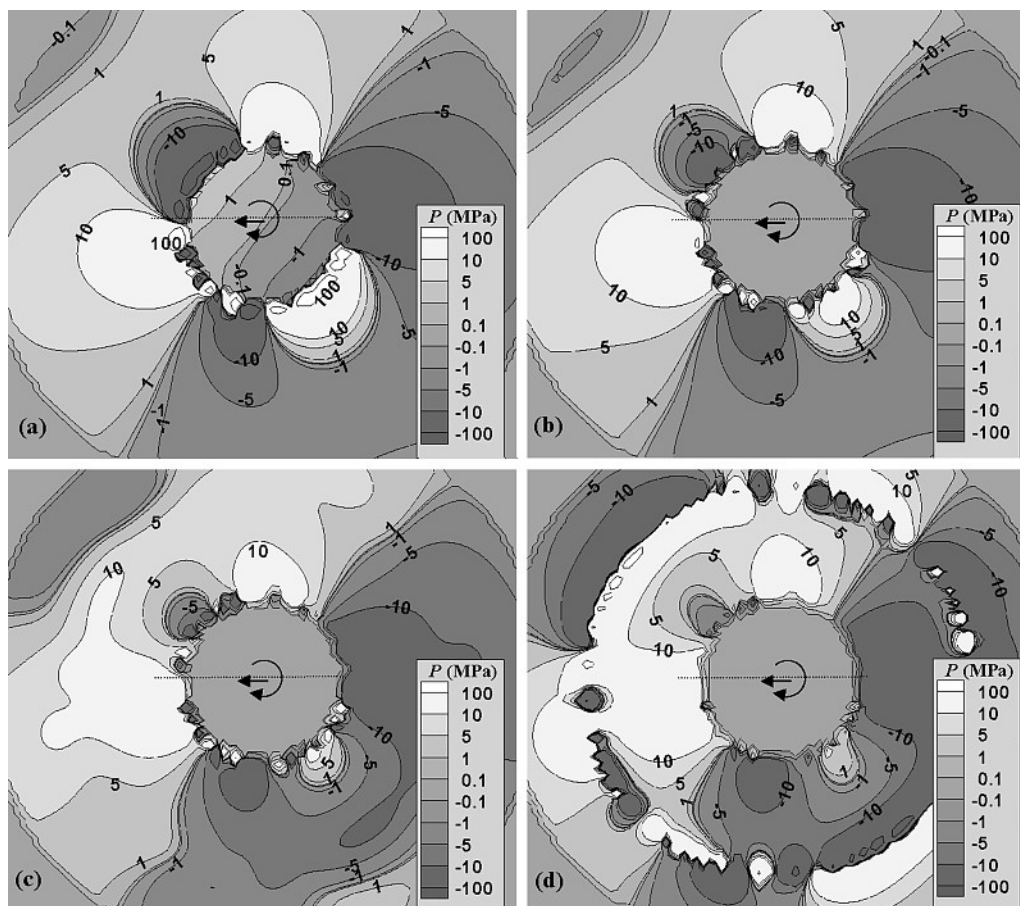


Fig. 10. Distribution of pressure around the tool at different elevations in the workpiece: (a)  $z = 1$  mm, (b)  $z = 3$  mm, (c)  $z = 5$  mm and (d)  $z = 7$  mm. The welding velocity was  $1.6 \text{ mm s}^{-1}$  and the rotational speed was 275 rpm.

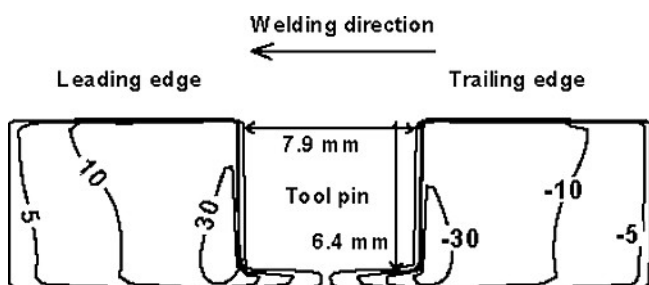


Fig. 11. Pressures are high in front of the tool, resisting tool motion. The welding velocity was  $1.6 \text{ mm s}^{-1}$  and the rotational speed was 275 rpm.

## References

- [1] W.M. Thomas, E.D. Nicholas, J.C. Needham, M.G. Church, P. Templesmith, C. Dawes, GB Patent No. 5460317 (1991).
- [2] W. Zhang, C.H. Kim, T. DebRoy: *J. Appl. Phys.* 95 (2004) 5210.
- [3] W. Zhang, C.H. Kim, T. DebRoy: *J. Appl. Phys.* 95 (2004) 5220.
- [4] C.H. Kim, W. Zhang, T. DebRoy: *J. Appl. Phys.* 94 (2003) 2667.
- [5] S. Mishra, T. DebRoy: *Acta Mater.* 52 (2004) 1183.
- [6] S. Mishra, T. DebRoy: *J. Phys. D: Appl. Phys.* 37 (2004) 2191.
- [7] K. Mundra, T. DebRoy, S.S. Babu, S.A. David: *Weld. J.* 76 (1997) S163.
- [8] T. Hong, W. Pitscheneder, T. DebRoy: *Sci. Technol. Weld. Joi.* 3 (1998) 33.
- [9] X. He, T. DebRoy, P.W. Fuerschbach: *J. Appl. Phys.* 94 (2003) 6949.
- [10] R. Miller, T. DebRoy: *J. Appl. Phys.* 68 (1990) 2045.
- [11] K. Mundra, T. DebRoy: *Metall. Trans. B* 24 (1993) 145.
- [12] M. Pastor, H. Zhao, R.P. Martukanitz, T. DebRoy: *Weld. J.* 78 (1999) 207s.
- [13] H. Zhao, T. DebRoy: *J. Appl. Phys.* 93 (2003) 10089.
- [14] H. Schmidt, J. Hattel, J. Wert: *Model. Simul. Mater. Sci.* 12 (2004) 143.
- [15] N. Kamp, A. Sullivan, J.D. Robson: *Mater. Sci. Eng., A* 466 (2007) 246.
- [16] R. Nandan, G.G. Roy, T.J. Lienert, T. DebRoy: *Acta Mater.* 55 (2007) 883.
- [17] R. Nandan, B. Prabu, A. De, T. DebRoy: *Weld. J.* 86 (2007) 313s.
- [18] R. Crawford, G.E. Cook, A.M. Strauss, D.A. Hartman, M.A. Stremmer: *Sci. Technol. Weld. Joi.* 11 (2006) 657.
- [19] R. Nandan, G.G. Roy, T. DebRoy: *Metall. Mater. Trans. A* 37 (2006) 1247.
- [20] G.G. Roy, R. Nandan, T. DebRoy: *Sci. Technol. Weld. Joi.* 11 (2006) 606.
- [21] R. Nandan, G.G. Roy, T.J. Lienert, T. DebRoy: *Sci. Technol. Weld. Joi.* 11 (2006) 526.
- [22] C.M. Chen, R. Kovacevic: *Int. J. Mach. Tool. Manu.* 43 (2003) 1319.
- [23] P.A. Colegrove, H.R. Shercliff: *Sci. Technol. Weld. Joi.* 8 (2003) 360.
- [24] P. Ulysse: *Int. J. Mach. Tool. Manu.* 42 (2002) 1549.
- [25] M.Z.H. Khandkar, J.A. Khan: *J Mater Process Manu* 10 (2001) 91.
- [26] A.P. Reynolds: *Mater. Sci. Forum* 519–521 (2006) 1095.
- [27] P.A. Colegrove, H.R. Shercliff: *Sci. Technol. Weld. Joi.* 11 (2006) 429.
- [28] A. De, T. DebRoy: *J. Phys. D: Appl. Phys.* 37 (2004) 140.
- [29] A. De, T. DebRoy: *J. Appl. Phys.* 95 (2004) 5230.
- [30] A. De, T. DebRoy: *Weld. J.* 84 (2005) 101s.
- [31] R. Storn, K. Price: *Journal of Global Optimization* 11 (1997) 341.
- [32] K. Price, R. Storn: *Dr Dobbs Journal* 22 (1997) 18.
- [33] O.C. Zienkiewicz, I.C. Corneau: *Arch. Mech.* 24 (1972) 873.
- [34] T. Sheppard, D.S. Wright: *Met. Technol.* 6 (1979) 215.
- [35] S. Bruschi, S. Poggio, F. Quadri, M.E. Tata: *Mater. Lett.* 58 (2004) 3622.
- [36] <http://aries.ucsd.edu/LIB/PROPS/PANOS/w.html>
- [37] R. Boyer, G. Welsch, E.W. Collings: *Materials properties handbook: Titanium alloys*, ASM International, Materials Park OH (1994).

- [38] H.S. Carslaw, J.C. Jaeger: Conduction of Heat in Solids, Clarendon Press, Oxford (1959).
- [39] T.J. Lienert, W.L. Stellwag, B.B. Grimmett, R.W. Warke: Weld. J. 82 (2003) 1S.
- [40] R. Schuhmann: Metallurgical Engineering, Addison-Wesley Press (1952).
- [41] S.V. Patankar: Numerical Heat Transfer and Fluid Flow, Hemisphere Publishing Corporation, New York (1980).
- [42] Z. Deng, M.R. Lovell, K.A. Tagavi: J. Manuf. Sci. Engg.-Trans. A.S.M.E 123 (2001) 647.
- [43] H.S. Kong, M.F. Ashby: M.R.S. Bulletin 16 (1991) 41.
- [44] M.Z.H. Khandkar, J.A. Khan, A.P. Reynolds: Sci. Technol. Weld. Joi. 8 (2003) 165.
- [45] A.I. Kahveci, G.E. Welsch: Scri. Metall. Mater. 20 (1986) 1287.

(Received November 10, 2007; accepted January 27, 2008)

#### Bibliography

DOI 10.3139/146.101655  
Int. J. Mat. Res. (formerly Z. Metallkd.)  
99 (2008) 4; page 434–444  
© Carl Hanser Verlag GmbH & Co. KG  
ISSN 1862-5282

#### Correspondence address

T. DebRoy  
Professor of Materials Science and Engineering  
115 Steidle Bldg, Pennsylvania State University, University Park  
PA 16802, USA  
Tel.: +1 814 865 1974  
E-mail: debroy@psu.edu

You will find the article and additional material by entering the document number MK101655 on our website at [www.ijmr.de](http://www.ijmr.de)